First Indirect Drive Experiment Using a Six-Cylinder-Port Hohlraum

Xin Li,[1] Yunsong Dong,[2] Dongguo Kang,[1] Wei Jiang,[2] Hao Shen,[1] Longyu Kuang,[2] Huasen Zhang,[1,*] Jiamin Yang,[2,†] Qiang Wang,[1] Chuansheng Yin,[2] Tianxuan Huang,[2] Wenyong Miao,[2] Zhongjing Chen,[2] Qi Tang,[2] Xiaoshi Peng,[2] Zifeng Song,[2] Xing Zhang,[2] Jianjun Dong,[2] Bo Deng,[2] Keli Deng,[2] Qiangqiang Wang,[2] Yimeng Yang,[2] Xiangming Liu,[2] Longfei Jing,[2] Hang Li,[2] Zhongjie Liu,[2] Bo Yu,[2] Ji Yan,[2] Yudong Pu,[2] Shaoyong Tu,[2] Yongteng Yuan,[2] Dong Yang,[2] Feng Wang,[2] Wei Zhou,[2] Xiaoxia Huang,[2] Zhibing He,[2] Haijun Zhang,[2] Yiyang Liu,[2] Shiyang Zou,[1] Baohan Zhang,[2] Yongkun Ding,[1] Shaoping Zhu,[1] and Weiyan Zhang[2]

[1]*Institute of Applied Physics and Computational Mathematics, Beijing 100088, China*

[2]*Research Center of Laser Fusion, Mianyang 621900, China*

(Received 6 December 2021; revised 30 March 2022; accepted 8 April 2022; published 9 May 2022)

The new hohlraum experimental platform and the quasi-3D simulation model are developed to enable the study of the indirect drive experiment using the six-cylinder-port hohlraum for the first time. It is also the first implosion experiment for the six laser-entrance-hole hohlraum to effectively use all the laser beams of the laser facility that is primarily designed for the cylindrical hohlraum. The experiments performed at the 100 kJ Laser Facility produce a peak hohlraum radiation temperature of ∼222 eV for ∼80 kJ and 2 ns square laser pulse. The inferred x-ray conversion efficiency $\eta \sim 87\%$ is similar to the cylindrical hohlraum and higher than the octahedral spherical hohlraum at the same laser facility, while the low laser backscatter is similar to the outer cone of the cylindrical hohlraum. The hohlraum radiation temperature and M-band (>1.6 keV) flux can be well reproduced by the quasi-3D simulation. The variations of the yield-over-clean and the hot spot shape can also be semiquantitatively explained by the calculated major radiation asymmetry of the quasi-3D simulation. Our work demonstrates the capability for the study of the indirect drive with the six-cylinder-port hohlraum at the cylindrically configured laser facility, which is essential for numerically assessing the laser energy required by the ignition-scale six-cylinder-port hohlraum.

DOI: 10.1103/PhysRevLett.128.195001

In inertial confinement fusion [1], a spherical capsule filled with deuterium and tritium fuel is imploded at high velocity ($300 - 400$ km/s). The compressed capsule consists of a low-density and high-temperature hot spot surrounded by a high-density and low-temperature shell. The thermonuclear ignition occurs when the central hot spot achieves the ignition condition expressed by the Lawson criterion [2] or its similar forms [3,4]. The imploding capsule is usually driven by either intense laser beams (direct drive) [5] or soft x rays produced by laser irradiation of a high-Z hohlraum (indirect drive) [6].

Conventionally, the cylindrical hohlraum with two laser entrance holes (LEHs) is used to convert laser energy into x rays for indirect drive [6], which naturally has even modes asymmetry described by the Legendre P_n modes. The current laser facilities, such as the National Ignition Facility (NIF) [7] and the 100 kJ Laser Facility [8,9], are primarily designed for the cylindrical hohlraum with laser beams arranged into inner and outer beams to control the low mode radiation asymmetry. However, due to the complexity of the laser-plasma interaction (LPI) and the plasma status inside the hohlraum, the low mode radiation asymmetry was still one of the major obstacles for achieving ignition at NIF in the past twelve years [10]. Various tuning techniques, such as the cross beam energy transfer (CBET) [11], have been used to minimize the radiation asymmetry in the cylindrical hohlraum, which contributes to the great progress of the indirect drive at NIF. Recently, it is reported that the marginal ignition regime has been achieved at NIF with fusion yield ∼1.3 MJ [12].

Meanwhile, new hohlraum design is explored to improve the radiation symmetry, such as the rugby-shaped hohlraum [13], the Frustraum [14], and the I-Raum [15]. These designs still use two LEHs for the hohlraum and can be easily applied at the current laser facilities. Recently, the octahedral hohlraums with six LEHs are also proposed for indirect drive [16–19]. Theoretically, the six-LEH octahedral hohlraum, with P_2 radiation asymmetry naturally mitigated, has robustly better symmetry than the two-LEH hohlraum with respect to laser pointing errors, capsule offset, and laser energy imbalance [20–22]. No complex symmetry tuning techniques are needed for the octahedral hohlraum. The octahedral spherical (OS) hohlraum [16,17] and the six-cylinder-port (SCP) hohlraum [18,19] are two branches of the octahedral hohlraums, which have different hohlraum geometry and laser injection [22]. The SCP

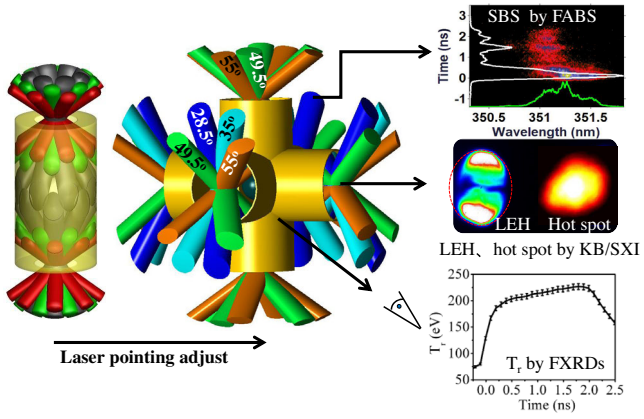

FIG. 1. The schematic scheme of the indirect drive experiment with the SCP hohlraum. The beams in orange (55°) and green (49.5°) are the outer beams of the cylindrical hohlraum, while the beams in blue (28.5°) and cyan (35°) are the inner beams.

hohlraum consists of six cylinder parts jointed like a six-way cross pipe (Fig. 1). For the ideal laser injection, the laser beams are incident in each LEH with the same angle to form a laser cone similar like the outer beams of the cylindrical hohlraum. The SCP hohlraum can provide similar excellent radiation symmetry and requires less laser energy compared to the OS hohlraum due to greater energy coupling efficiency [22]. It is also expected that significant stimulated Raman scattering (SRS) could be avoided for the SCP hohlraum at ignition-scale due to the absence of the inner beams.

It is essential to investigate the SCP hohlraum at the current laser facility to assess its performance at ignition-scale. Although the cylindrical hohlraum [6,23–25] and the OS hohlraum [26–28] have been intensively investigated, the SCP hohlraum is little investigated mainly because, first, the configuration of the current laser facility is primarily designed for the cylindrical hohlraum, not ideal for the SCP hohlraum. The laser pointing and hohlraum size should be designed together to ensure that the laser beams can be incident into the SCP hohlraum. Second, the geometry of the SCP hohlraum is three dimensional (3D). It is hard to infer the radiation drive to capsule without 3D simulation. Third, new techniques are needed for target fabrication since the current technique is mainly for the cylindrical hohlraum.

In this Letter, by developing the new hohlraum experimental platform at the 100 kJ Laser Facility, the indirect drive experiments with the six-LEH SCP hohlraum are performed for the first time. Figure 1 shows the laser pointing adjustment and the schematic scheme of the experiment with the SCP hohlraum. In the experiments with the cylindrical hohlraum (Fig. 1), the inner cone of each LEH side consists of four beams at 28.5° and four beams at 35° relative to the hohlraum axis. Meanwhile, eight beams at 49.5° and eight beams at 55° are injected into each LEH side to form the outer cone. In the current experiments with the SCP hohlraum, the laser pointing and the hohlraum size are designed correlatively to ensure that each LEH has eight beams incident. The SCP hohlraum has a diameter of 1.4 mm and a length of 3.4 mm in each direction. The LEH is fully opened to ensure that the laser beam can be incident into the hohlraum. For each LEH in the polar direction, four 49.5° and four 55° beams (outer beams of the cylindrical hohlraum) are incident to approximately form a cone. For the four LEHs in the equatorial direction, two 28.5° and two 35° beams (inner beams of the cylindrical hohlraum) are incident in each LEH along with two 49.5° and two 55° beams. The incident angles relative to its own cylinder axis are 62.1°, 61.5°, 47.9°, and 50.7°, respectively. In this case, all the 48 laser beams of the cylindrically configured laser facility can be effectively used for the six-LEH hohlraum for the first time, while the OS hohlraum only uses 32 laser beams unequally injected to the six LEHs [27,28]. Four flat response x-ray detectors (FXRDs) [29] and M-band (1.6 to 4.4 keV) flat-response x-ray detector (MXRDs) [30] are used to measure the time-resolved radiation flux F and the M-band flux at different view angles. The radiation temperature (T_r) is calculated by $T_r^4 = F/\mathrm{sum}(\sigma A_{\mathrm{LEH}} \cos\theta_i)$. Here, A_{LEH} is the area of the LEH. θ_i is the polar angle between the ith LEH and the FXRD. σ is the Stefan-Boltzmann constant. The stimulated Brillouin scattering (SBS) and the SRS are measured by the full aperture backscatter station [31]. The Kirkpatrick-Baez (KB) microscope is used to measure the time-integrated self-emission shape of the hot spot. The time-integrated image of the hohlraum interior and the LEH are recorded with the static x-ray imager, which indicates that the laser beams can be fully injected into the LEHs.

A series of implosion experiments are performed using both vacuum and gas-filled SCP hohlraums. The gas-filled hohlraum is filled with 0.4 atm neopentane (C_5H_{12}). In the experiment, each laser beam delivers a 2 ns square laser pulse. The incident laser energy is from $E_l = 76$ kJ to $E_l = 86$ kJ. Figure 2(a) shows the measured peak T_r. The overall peak T_r varies from 220 to 230 eV for different FXRDs due to the different viewed area of the LEHs, capsule, and laser spots. The measured T_r is about 40 eV higher than the OS hohlraum [27], mainly because the SCP hohlraum has higher laser power, higher x-ray conversion efficiency, and smaller hohlraum wall area. Since the FXRD-3 views only the hohlraum wall and does not view the capsule or the other LEHs, the T_r of FXRD-3 is more appropriate to represent the overall hohlraum T_r. It is indicated by the FXRD-3 that the T_r of the SCP hohlraum is about 222 eV for $E_l^{\mathrm{net}} = 80$ kJ. Here, E_l^{net} is the net incident laser energy excluding the backscattered laser energy. The laser backscatter is dominated by SBS. The backscatter fraction is about 2% and 5% for the vacuum and gas-filled hohlraums, respectively. The laser backscatter property is similar to the outer beams of the cylindrical hohlraum at the same laser facility.

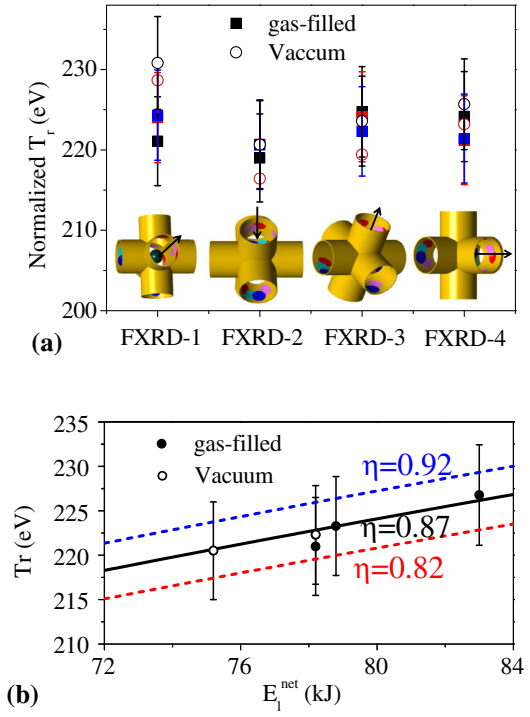

FIG. 2. (a) The normalized peak T_r by the FXRDs with view sight shown at the bottom. The different colored symbols represent different shots. The laser spots on the wall are shown by the colored spots. The polar direction is shown by the black arrows. Here, T_r is normalized to $E_l^{\rm net} = 80$ kJ by $T_r = (80\ {\rm kJ}/E_l^{\rm net})^{0.25} T_r^{\rm exp}$. (b) The peak T_r versus $E_l^{\rm net}$ for FXRD-3. The error bar of the T_r is ±2.5%.

The x-ray conversion efficiency of the SCP hohlraum is further assessed using the power balance equation

$$\eta(P_L - P_s) = [(1-\alpha_w)A_w + (1-\alpha_{\rm cap})A_{\rm cap} + A_{\rm LEH}]\sigma T_r^4 .$$

Here, P_L and P_s are the incident and backscattered laser power, respectively. A_w is the area of the hohlraum wall and $A_{\rm cap}$ is the area of the capsule. α_w and $\alpha_{\rm cap}$ are the albedo of the hohlraum wall and the capsule, respectively. For the current experimental parameters, $\alpha_w = 0.89$ is used similar like in Ref. [25] and $\alpha_{\rm cap} = 0.3$ since the laser pulse shape and the beam power are quite similar for the two experiments. The inferred x-ray conversion efficiency is $\eta \sim 87 \pm 5\%$ for both vacuum and gas-filled SCP hohlraum [Fig. 2(b)], similar to the cylindrical hohlraum [25] and higher than $\eta \sim 80\%$ of the OS hohlraum [27] at the laser facility. We speculate that the SCP hohlraum may have similar x-ray conversion efficiency as the cylindrical hohlraum at ignition-scale while the laser backscatter by SRS may be significantly reduced since the laser-wall interaction for the SCP hohlraum is similar to the outer beams of the cylindrical hohlraum.

The hohlraum radiation field is further investigated by the quasi-3D simulation model. Here, "quasi-3D" means

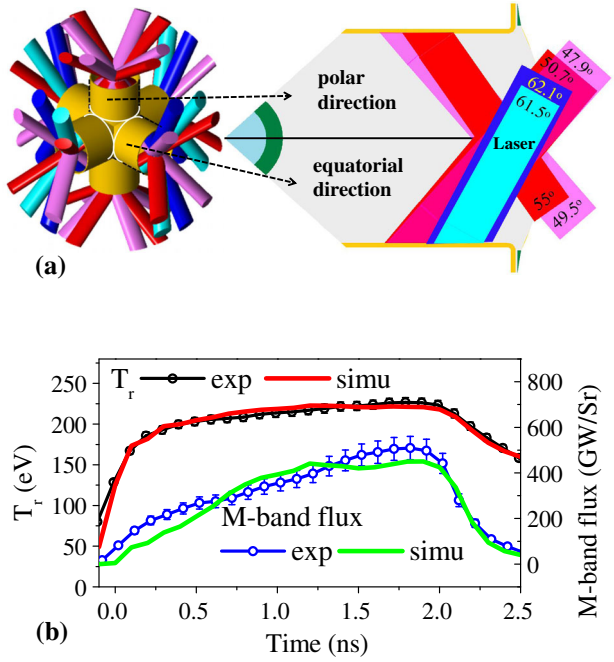

FIG. 3. (a) The schematic scheme of the quasi-3D simulation. The laser incident angle and the laser trajectory are also shown. (b) Comparisons of the T_r and the M-band flux between the experiment and the simulation for N166.

that the 3D hohlraum radiation field is constructed based on a series of 2D simulations. In the quasi-3D simulation, the SCP hohlraum is divided into six cylindrical parts with axial symmetry [Fig. 3(a)]. Each cylindrical part is simulated separately by the 2D radiation hydrodynamic code LARED [32]. In each 2D simulation, the laser energy of the same incident angle is equally divided to the 2D laser cone with the same pointing region. The reflected boundary condition is used for the joint region inside the hohlraum. The 3D radiation field of the whole SCP hohlraum is approximately constructed by jointing the six cylindrical parts together. It should be noted that a small piece of the connecting region [white regions in Fig. 3(a)] are not included in the quasi-3D simulation model. Since the area of the missing regions is only about 3.6% of the whole hohlraum area, it affects little of the overall hohlraum energy. When constructing the whole hohlraum radiation field, the plasma status of these regions is extrapolated from

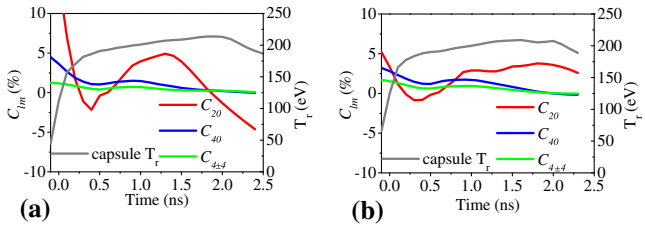

FIG. 4. The postprocessed capsule T_r and radiation asymmetry for N166 (a) and N176 (b).

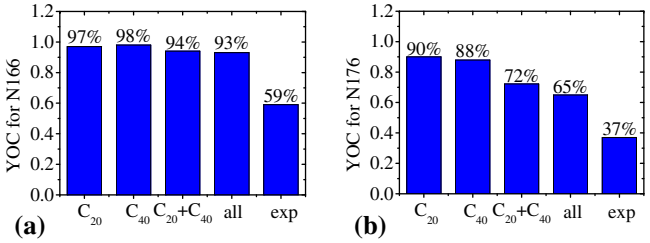

FIG. 5. The yield degradation by radiation asymmetry for N166 (a) and N176 (b).

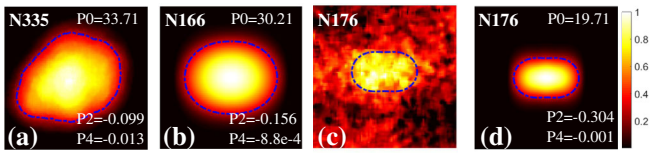

FIG. 6. The equatorial hot spot self-emission images from the experiments [(a) and (c)] and simulations [(b) and (d)]. The dashed lines are the 30% contour. The 30% contour in panel (d) is overplotted on panel (c) since the noise level is too significant to analyze the asymmetry.

the simulated regions. The shot N20180705166 (N166) is used as an example to show the validity of the quasi-3D simulation on describing the radiation field of the SCP hohlraum [Fig. 3(b)]. It is shown that the postprocessed T_r and the M-band flux for FXRD-3 agree with the experiment except for the slight disagreement of M-band flux before 0.5 ns. Similar results are also found for the other shots, indicating that the quasi-3D simulation is valid to describe the radiation field inside the SCP hohlraum.

Next, the implosion performance is investigated by the 2D capsule-only simulations using the constructed radiation drive. Two typical shots N166 and N20180710176 (N176) are simulated and compared with the experiments. The shot N166 uses the gas-filled hohlraum. The capsule consists of 28.1 μm thick plastic ablator filled with 9.6 atm DD gas inside the radius of 307.7 μm. The shot N176 uses the vacuum hohlraum. The capsule consists of 49.9 μm thick plastic ablator filled with 5.6 atm DD gas inside the radius of 309.5 μm. The convergence ratio is Cr $\sim$ 10 for N166 and is Cr $\sim$ 20 for N176, which means that N176 is more sensitive to radiation asymmetry than N166. Figure 4 shows the capsule T_r and the radiation asymmetry from the quasi-3D simulation. For the SCP hohlraum, the 3D radiation asymmetry on the capsule is described by the spherical harmonic expansion $F = \sum_{l=0}^{\infty}\sum_{m=-l}^{m=l} a_{lm}Y_{lm}(\theta,\varphi)$ with a_{lm} the spherical harmonic decomposition. The relative asymmetry is defined as $C_{l0} = |a_{l0}|/a_{00}$ and $C_{lm} = |a_{lm}|/a_{00}$. For the current nonideal laser injection, it is found that C_{20}, C_{40}, and $C_{4\pm4}$ are the major asymmetry components. C_{20} and C_{40} are 2D asymmetry components while $C_{4\pm4}$ is a 3D asymmetry component. It is shown that the evolution of C_{40} and $C_{4\pm4}$ are quite similar between the gas-filled hohlraum and the vacuum hohlraum. The value of C_{40} is about 1.8× larger than $C_{4\pm4}$. In the gas-filled hohlraum, C_{20} reaches a peak value of 5% around 1.3 ns and decreases to negative. In the vacuum hohlraum, C_{20} sustains around 3.5% from 1 to 2 ns.

The performance degradation by radiation asymmetry is summarized in Fig 5. Since the $C_{4\pm4}$ radiation asymmetry cannot be self-consistently considered in the 2D simulation, it is effectively considered by adding it to C_{40} through $C_{40}^{\text{eff}} = \sqrt{C_{40}^2 + 2C_{4\pm4}^2}$ similar to that in Ref. [33]. For shot N166, the experimental neutron yield is 1.69×10^9. The yield-over-clean (YOC) is $\text{YOC}_{1\text{D}} = 59\%$ [Fig. 5(a)], which is close to the cylindrical hohlraum implosions with the same Cr at the 100 kJ Laser Facility [34]. The yield degradation by radiation asymmetry is small due to small Cr. By taking into account all the radiation asymmetry components in Fig. 3(a), the yield of the 2D simulation is about 93% of that in 1D. Therefore, the 2D YOC with radiation asymmetry is $\text{YOC}_{2\text{D sym}} = 63\%$. For shot N176, the experimental neutron yield is 1.0×10^9 and the $\text{YOC}_{1\text{D}} = 37\%$. By taking into account all the radiation asymmetry in Fig. 3(b), the yield of the 2D simulation is about 65% of that in 1D, which is more degraded than N166 due to larger Cr [Fig. 5(b)]. The 2D YOC is $\text{YOC}_{2\text{D sym}} = 60\%$ for N176 and is similar as the 2D YOC for N166. Overall, the variation of $\text{YOC}_{1\text{D}}$ between N166 and N176 can be semiquantitatively explained by the yield degradation of the major radiation asymmetry if all other degradation contributions were equal. Other effects should also be assessed to fully understand the yield degradation.

The hot spot shape is also compared between the experiments and the simulations (Fig. 6). The shot N20191227335 (N335) is a repeat of N166 but with 0.3% Ar filled in the capsule to enhance the self-emission signal. Therefore, the image of N335 is less noisy than N176. It is shown that the experimental hot spot shape is more deviated from 1D in N176 than that in N335. The variation of the hot spot shape between the two shots can also be semiquantitatively explained by the calculated major radiation asymmetry of the quasi-3D model, indicating that the quasi-3D model can roughly describe the major radiation asymmetry.

In summary, a new experimental platform is developed at the 100 kJ Laser Facility to enable the study of the indirect drive implosion using the SCP hohlraum and all the 48 laser beams. The experiments produce a peak radiation temperature of ~222 eV for the ~80 kJ and 2 ns square laser pulse. It is found that the inferred x-ray conversion efficiency is $\eta \sim 87\%$, similar to the cylindrical hohlraum and higher than the OS hohlraum at the same laser facility. The laser backscatter is dominated by SBS with its fraction similar like the outer beams of the cylindrical hohlraum. A quasi-3D simulation model is developed to investigate the radiation field of the SCP hohlraum. The simulated T_r

and M-band flux are consistent with the experiments. The variation of the YOC_{1D} and the hot spot shape can also be semi-quantitatively explained by the calculated major radiation asymmetry. Our Letter supports the assessing that the ignition-scale SCP hohlraum with robustly high radiation symmetry can be driven by about 2 MJ laser energy [18,22].

We thank the laser facility operation and target fabrication collaborators at the Laser Fusion Research Center (LFRC), as well as the external collaborators at Tongji University for KB diagnostics. This work was funded by the National Key R&D program under Contract No. 2017YFA0403204, the National Natural Science Fund of China under Contracts No. 11435011, No. 11975056, and the Laser Fusion Research Center Funds for Young Talents under Contract No. RCFPD1-2017-1.

X. L. and Y. D. contributed equally to this work.

*zhang_huasen@hotmail.com
†yjm70018@sina.cn

[1] S. Atzeni and J. Meyer-ter-Vehn, *The Physics of Inertial Fusion* (Clarendon, Oxford, 2004).
[2] J. D. Lawson, Proc. Phys. Soc. London Sect. B **70**, 6 (1957).
[3] B. K. Spears, S. Glenzer, M. J. Edwards, S. Brandon, D. Clark, R. Town, C. Cerjan, R. Dylla-Spears, E. Mapoles, D. Munro *et al.*, Phys. Plasmas **19**, 056316 (2012).
[4] C. D. Zhou and R. Betti, Phys. Plasmas **15**, 102707 (2008).
[5] R. S. Craxton, K. S. Anderson, T. R. Boehly, V. N. Goncharov, D. R. Harding, J. P. Knauer, R. L. McCrory, P. W. McKenty, D. D. Meyerhofer, J. F. Myatt *et al.*, Phys. Plasmas **22**, 110501 (2015).
[6] J. D. Lindl, P. Amendt, R. L. Berger, S. G. Glendinning, S. H. Glenzer, S. W. Haan, R. L. Kauffman, O. L. Landen, and L. J. Suter, Phys. Plasmas **11**, 339 (2004).
[7] E. I. Moses, J. D. Lindl, M. L. Spaeth, R. W. Patterson, R. H. Sawicki, L. J. Atherton, P. A. Baisden, L. J. Lagin, D. W. Larson, B. J. MacGowan *et al.*, Fusion Sci. Technol. **69**, 1 (2016).
[8] X. T. He and W. Y. Zhang, Eur. Phys. J. D **44**, 227 (2007).
[9] W. Zheng, X. Wei, Q Zhu, F. Jing, D. Hu, J. Su, K. Zheng, X. Yuan, H. Zhou, W. Dai *et al.*, High Power Laser Sci. Eng. **4**, e21 (2016).
[10] D. A. Callahan, O. A. Hurricane, J. E. Ralph, C. A. Thomas, K. L. Baker, L. R. Benedetti, L. F. B. Hopkins, D. T. Casey, T. Chapman, C. E. Czajka *et al.*, Phys. Plasmas **25**, 056305 (2018).
[11] P. A. Michel, S. H. Glenzer, L. Divol, D. K. Bradley, D. Callahan, S. Dixit, S. Glenn, D. Hinkel, R. K. Kirkwood, J. L. Kline *et al.*, Phys. Plasmas **17**, 056305 (2010).
[12] A. L. Kritcher, Initial results from the HYBRID-E DT experiment N210808 with >1.3 MJ yield, in *Proceedings of the International Conference on Inertial Fusion Sciences and Applications* (2021), https://www.llnl.gov/news/national-ignition-facility-experiment-puts-researchers-threshold-fusion-ignition.
[13] M. Vandenboomgaerde, J. Bastian, A. Casner, D. Galmiche, J. P. Jadaud, S. Laffite, S. Liberatore, G. Malinie, and F. Philippe, Phys. Rev. Lett. **99**, 065004 (2007).
[14] P. Amendt, D. Ho, Y. Ping, V. Smalyuk, S. Khan, J. Lindl, D. Strozzi, R. Tommasini, M. Belyaev, C. Cerjan, O. Jones, W. Kruer, N. Meezan, H. Robey, F. Tsung, C. Weber, and C. Young, Phys. Plasmas **26**, 082707 (2019).
[15] H. F. Robey, L. B. Hopkins, J. L. Milovich, and N. B. Meezan, Phys. Plasmas **25**, 012711 (2018).
[16] K. Lan, X. T. He, J. Liu, W. D. Zheng, and D. X. Lai, Phys. Plasmas **21**, 052704 (2014).
[17] K. Lan and W. D. Zheng, Phys. Plasmas **21**, 090704 (2014).
[18] X. Li, C. S. Wu, Z. S. Dai, W. D. Zheng, J. F. Gu, P. J. Gu, S. Y. Zou, J. Liu, and S. P. Zhu, Chin. Phys. B **25**, 085202 (2016).
[19] L. Y. Kuang, H. Li, L. F. Jing, Z. W. Lin, L. Zhang, L. L. Li, Y. K. Ding, S. E. Jiang, J. Liu, and J. Zheng, Sci. Rep. **6**, 34636 (2016).
[20] W. Y. Huo, J. Liu, Y. Q. Zhao, W. D. Zheng, and K. Lan, Phys. Plasmas **21**, 114503 (2014).
[21] H. Duan, C. S. Wu, W. B. Pei, and S. Y. Zou, Phys. Plasmas **22**, 092704 (2015).
[22] L. Jing, S. Jiang, L. Kuang, H. Li, L. Zhang, L. Li, Z. Lin, J. Zheng, Y. Huang, T. Huang, and Y. Ding, Nucl. Fusion **58**, 096017 (2018).
[23] J. D. Lindl, O. Landen, J. Edwards, E. Moses, and NIC team, Phys. Plasmas **21**, 020501 (2014).
[24] J. L. Kline, S. H. Glenzer, R. E. Olson, L. J. Suter, K. Widmann, D. A. Callahan, S. N. Dixit, C. A. Thomas, D. E. Hinkel, E. A. Williams *et al.*, Phys. Rev. Lett. **106**, 085003 (2011).
[25] H. Zhang, W. Jiang, F. Ge, P. Song, S. Zou, T. Huang, S. Li, D. Yang, Z. Li, L. Hou *et al.*, Phys. Plasmas **25**, 022703 (2018).
[26] K. Lan, J. Liu, Z. Li, X. Xie, W. Huo, Y. Chen, G. Ren, C. Zheng, D. Yang, S. Li *et al.*, Matter Radiat. Extremes **1**, 8 (2016).
[27] W. Y. Huo, Z. Li, Y.-H. Chen, X. F. Xie, G. L. Ren, H. Cao, S. Li, K. Lan, J. Liu, Y. Li *et al.*, Phys. Rev. Lett. **120**, 165001 (2018).
[28] K. Lan, Y. S. Dong, J. F. Wu, Z. C. Li, Y. H. Chen, H. Cao, L. Hao, S. Li, G. L. Ren, W. Jiang *et al.*, Phys. Rev. Lett. **127**, 245001 (2021).
[29] Z. Li, X. Jiang, S. Liu, T. Huang, J. Zheng, J. Yang, S. Li, L. Guo, X. Zhao, H. Du *et al.*, Rev. Sci. Instrum. **81**, 073504 (2010).
[30] Liang Guo, S. W. Li, J. Zheng, Z. C. Li, D. Yang, H. B. Du, L. F. Huo, Y. L. Cui, J. M. Yang, S. Y. Liu *et al.*, Meas. Sci. Technol. **23**, 065902 (2012).
[31] S. Jiang, F. Wang, Y. Ding, S. Liu, J. Yang, S. Li, T. Huang, Z. Cao, Z. Yang, X. Hu *et al.*, Nucl. Fusion **59**, 032006 (2019).
[32] W. Pei, Commun. Comput. Phys. **2**, 255 (2007).
[33] W. J. Krauser, N. M. Hoffman, D. C. Wilson, B. H. Wilde, W. S. Varnum, D. B. Harris, F. J. Swenson, and P. A. Bradley, Phys. Plasmas **3**, 2084 (1996).
[34] Y. Pu, T. Huang, F. Ge, S. Zou, F. Wang, J. Yang, S. Jiang, and Y. Ding, Plasma Phys. Controlled Fusion **60**, 085017 (2018).